Available online at www.sciencedirect.com

jmr&t Journal of Materials Research and Technology

journal homepage: www.elsevier.com/locate/jmrt

Original Article

Influences of SiO_2, Al_2O_3, CaO and MgO in phase transformation of sintered kaolin-ground granulated blast furnace slag geopolymer

Noorina Hidayu Jamil [a,*], *Mohd. Mustafa Al Bakri Abdullah* [a], *Faizul Che Pa* [a], *Hasmaliza Mohamad* [b], *Wan Mohd Arif W. Ibrahim* [a], *Jitrin Chaiprapa* [c]

[a] *Center of Excellence Geopolymer and Green Technology, School of Materials Engineering, Universiti Malaysia Perlis, 01000, Perlis, Malaysia*

[b] *Biomaterial Research Niche Group, School of Materials and Mineral Resources Engineering, Universiti Sains Malaysia, 14300, Nibong Tebal, Penang, Malaysia*

[c] *Synchrotron Light Research Institute, Muang, Nakhon Ratchasima, 3000, Thailand*

ARTICLE INFO

Article history:
Received 3 July 2020
Accepted 15 October 2020
Available online 22 October 2020

Keywords:
Kaolin
GGBS
Sintering geopolymer

ABSTRACT

Kaolin has an excellent structure formed via a wide range of firing temperature. The correlation between the mineralogy and reactivity of individual elements is extremely complex in a sintered geopolymer material. The main objective of this work is to elucidate the influence of the chemical composition of the raw materials used post-sintering on the kaolin-ground granulated blast furnace slag (GGBS) geopolymer. The samples were cured at room temperature for 5 days before being sintered. The ratio of solid-to-liquid were 1:1, 1.5:1, and 2:1. The addition of the GGBS to the kaolin geopolymer slurry did not only hasten the hardening process during geopolymerization, the presence of SiO_2, Al_2O_3, CaO, and MgO in GGBS had accelerated the formation of nepheline, gehlenite, akermanite, and albite phase after sintering based on the result from x-ray diffraction and fourier-transform infrared spectroscopy On top of the phase transformation, a high ratio of solid-to-liquid (SL 2) had improved the pore distribution from irregular size to well defined formation and increased the densification of the sintered materials. Elemental distribution from micro-XRF investigation prove the high concentration of Ca in localized area and uniformly distribution of Si aligned with the phase of akermanite in SL 2. The main chemical composition of kaolin and GGBS which are SiO_2, Al_2O_3, CaO and MgO had contributed in phase transformation of sintered kaolin-GGBS geopolymer.

* *Corresponding author.*
E-mail address: noorinahidayu@unimap.edu.my (N.H. Jamil).

https://doi.org/10.1016/j.jmrt.2020.10.045

1. Introduction

Environmental preservation has become a driving force behind the search for new sustainable and environmentally friendly materials. The development of geopolymer glass-ceramic has become an attractive research topic due to the low energy consumption required during the production process relative to conventional approaches [1–3]. Conventional approaches of sintering glass-ceramics usually include two steps; vitrifying raw materials at high temperatures (1300 °C –1500 °C), followed by nucleation and crystal growth [2]. Difficulty vitrifying the raw materials is one of the limitations in the conventional route due to its high energy consumption. Alternative manufacturing techniques have been proposed involving fine glass powders being pressed and sintered, which addresses the drawbacks of conventional techniques. However, this approach requires a short time to vitrify raw materials at high temperatures for the preliminary glass-making step [2,4]. Whilst, direct sintering of geopolymer material at high temperatures will result in excessive shrinkage and cracking of the geopolymers [5]. Hence, the method to sinter geopolymeric materials in order to produce geopolymer glass-ceramic at lower sintering temperature still remain as a challenge and attract many researchers.

The geopolymerization process of raw materials resulted in the formation of amorphous to sub-crystalline spatial structures [6,7]. It is believed that the chemical composition of the source material influences the phase transformation of the sintered geopolymer alongside other factors such as solid-to-liquid ratios, concentration of sodium hydroxide (NaOH), and curing condition [8]. The most used raw materials are natural minerals, such as calcined clays, and industrial wastes, such as fly ash, slag, red mud, and waste glass. It was reported that the appropriate concentration of NaOH that can be used to synthesize kaolin geopolymer were 6M–8M [9,10]. This range of molarity already enough to provide the alkalinity condition for Al [Al6] changed to [Al4] since this coordination number of [Al4] was required in geopolymerization process [11].

Research reported the contribution of the chemical compositions in geopolymers via what is called the backbone. The structure of a geopolymer consists of polymeric Si–O–Al framework tetrahedral, with shared oxygen forming 3-D network, and metal cations (sodium, potassium, lithium, or calcium) and bound water molecules stabilizing the structure [6,12]. In order to maintain strong framework bonding, Na–K bond should be avoided [13]. Aluminium (Al) plays a significant role in ensuring the long-term durability of the geopolymers [14]. However, it is believed that in order to achieve a high chemical interaction of kaolin during the production process, more time is required due to the slow dissolution rate of the Al content [15].

Few studies reported the use of kaolin as a raw material in geopolymers, however, more can be found on the use of metakaolin to produce geopolymers [16–18]. In order to decrease energy usage during production, kaolin as a source of aluminosilicate material can be used without pre-treatments for preparing geopolymers (Hounsi et al., 2014). Some studies outlined that kaolin geopolymers can be manufactured using different additives, such as bagasse and rice husk ash [19,28].

The use of blast furnace slag has been reported, mainly consisting of CaO, SiO_2, Al_2O_3, and MgO. The use of such materials as glass sources to produce sintered glass–ceramics excludes the step of vitrifying raw materials at high-temperatures [4,20,27]. The presence of Ca^{2+} in the geopolymeric system can significantly influence the formation of what is called geopolymer gels due to the Ca^{2+} encouraging the formation of crystalline phases at high temperatures [20]. CaO from slag act as a setting agent, which leads to hardened at room temperature without affecting the mechanical properties of the final product [8]. [29] Hongyu (2009) was used limestone as source of CaO to form fine glass of vitreous Ca–Al–Mg silicate, which excluded vitrification at high temperature.

This study intends to investigate the chemical composition in kaolin-GGBS geopolymer towards phase transformation after sintering. The ground-granulated blast furnace slag was added with kaolin and activated via a combination of alkaline solution prepared using sodium silicate and sodium hydroxide. In order to elucidate the reactions of sintered geopolymer, the solid-to-liquid ratio (binder-to-activator solution) was varied.

2. Materials and methods

2.1. Starting materials

The kaolin was obtained from the Associated Kaolin Industries Sdn. Bhd., Malaysia, and used as the main source of aluminosilicate to make the geopolymer material. Ground-granulated blast furnace slag (hereafter referred to as GGBS) was used as an additive. A mixture of sodium silicate (Na_2SiO_3) and sodium hydroxide (NaOH) solutions were used as an alkali activator during geopolymerization. The NaOH solution was prepared in a volumetric flask and cooled to room temperature with a constant molarity (8M) for all of the mixtures. The chemical composition of the Na_2SiO_3 solution was ~30.1% for SiO_2, ~9.4% for Na_2O, and ~60.5% for H_2O. The mixture of kaolin and GGBS will hereafter be referred to as solid, while alkali activator will be referred to as liquid.

2.2. Kaolin-GGBS geopolymer mixture proportions

The geopolymer samples were made from kaolin, with GGBS as an additive at a fixed ratio of 4:1 wt.%. NaOH was mixed with Na_2SiO_3 at a fixed ratio of Na_2SiO_3 to NaOH of 4:1 to prepare an alkali activator solution 24h prior to use. Kaolin was mixed with the alkali activator until it becomes a slurry using a mechanical stirrer. Then, GGBS was added and the mixing continued until the slurry was homogenized and ready to be poured into a 50 × 50 × 50 mm steel mould (~10% of distilled water was added for the 1.5 and 2 ratios to decrease the viscosity). The slurry was vibrated to remove trapped air, then sealed with plastic at the exposed portion of the mould during the curing stage. Samples were cured at room temperature for 5 days and demoulded afterwards. The cured samples were sintered at a heating profile shown in Fig. 1. The

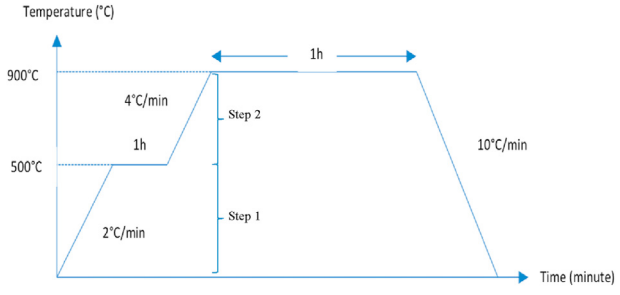

Fig. 1 – Two-steps sintering profile of kaolin-GGBS geopolymer.

sintered kaolin-GGBS geopolymer were labelled based on its solid-to-liquid ratios, which are SL 1 (solid-to-liquid ratio of 1:1), SL 1.5 (solid-to-liquid ratio of 1.5:1), and SL 2 (solid-to-liquid ratio of 2:1).

2.3. *Characterization*

Kaolin and GGBS, as sources of aluminosilicate, had its particle size distribution measured using a particle size analyzer (MASTERSIZER 3000) at a rotating speed at 2500 rpm, with distilled water as its dispersion medium. Its chemical compositions were determined using X-Ray Fluorescence (XRF). The thermal behaviour of both materials were evaluated using a Differential Scanning Calorimetry – Thermogravimetric analysis (DSC -TGA) (METTLER TOLEDO) at a heating rate of ~10 °C/min up to 1200 °C using Pt-crucible. The phase composition of the raw materials and sintered kaolin-GGBS geopolymer were determined using the X-ray diffraction method (XRD) (BRUKER D8 ADVANCE), equipped with a copper anode (Cu Ka, λ 1.5406 Å). Prior to analysis, dry powder were compacted and analysis were recorded within a 2θ range of 5 - 80°, with a scan rate 0.1 s/s and the data analysed using the X'Pert HighScore Plus software. Fourier transform infrared spectroscopy (FTIR) (PERKIN ELMER SPECTRUM ONE) was utilized to identify the structural surface of the raw materials and the sintered kaolin-GGBS geopolymer within 400–1400 cm^{-1}. Potassium bromide (KBr) powder was mixed with glass powder within an agate mortar at a ratio of 9:1. The powder mixture was pressed into a transparent pellet form with a diameter of <5 mm using a hand press machine. The microstructure was imaged using a Scanning Electron Microscope (SEM) and elemental analysis (EDX) (ZeissSupra 35VP) which worked at an accelerating voltage of 5 kV. The specimens were cut into small pieces and grind to obtain a flat surface. The samples were vacuumed for an hour and coated with Au–Pd on its surface for imaging purposes.

The distribution of elements was assessed by using synchrotron μ-XRF at BL6b beamline at the Synchrotron Light Research Institute (SLRI), Thailand. The continuous synchrotron radiation was focused by a polycapillary lens to establish a micro X-ray beam (beam size of 30 μm × 30 μm) on the samples. The energy of micro X-ray beam was set between 2 and 12 keV without monochromator feature. The samples were mounted vertically on the holder, while raster scanning was performed by using high precision motorised stages. The experiments were conducted in helium gas atmosphere and the exposure time for each point was 30 s. A total scan of 961 points was obtained with a detector dead time close to 20%, as described in [21]. The resultant images were created in bilinear interpolation and analysed using PyMca software.

3. Result and discussion

3.1. *Characterization of kaolin and GGBS*

Fig. 2 shows the difference of the particle size distribution between the kaolin and GGBS, where the particle size of the latter is much coarser than the former. The average particle size of kaolin is ~13.3 μm, while GGBS has a particle size of ~41.4 μm. Smaller particle size implies a larger surface area ideally, which means that despite kaolin's low reactivity as per the literature, its large surface area increases its overall surface contact with the GGBS, which is further enhanced via the use of the alkali activator utilized during the geopolymerization.

The general chemical composition of the kaolin and GGBS obtained from the XRF are shown in Table 1. Both reported its main chemical composition as being SiO_2 and Al_2O_3. Besides the main composition forming the framework, kaolin also consists of K_2O (~6.05%), which contribute flux that lowers the melting temperature. The large amount of flux in GGBS, which is the sum of CaO (~50.37%) and MgO (~3.2%), does not only reduce the sintering temperature, it also prompts the geopolymerization process. This chemical composition were act as self-fluxing component during ceramic sintering process. This is especially the case in SiO_2, which melts to form a glassy phase during sintering, which bonds it to the ceramic body. Flux can also promote vitrification (the formation of a glassy phase) at lower temperatures [2]].

The diffraction patterns of raw kaolin and GGBS are shown in Fig. 3. Kaolin consist of the crystalline phases kaolinite ($Al_4(OH)_8(Si_4O_{10})$), SiO_2, and fibroferrite ($Fe(OH)(SO_4)(H_2O)_5$). According to the semi-quantitative analysis, the kaolin used in this study is composed of ~88% $Al_4(OH)_8(Si_4O_{10})$, ~7% of SiO_2, and ~5% of $Fe(OH)(SO_4)(H_2O)_5$. The elements present in the phases of kaolin is reflected by the high percentage of chemical compositions, which are SiO_2, Al_2O_3, and Fe_2O_3. Ground granulated blast furnace slag contains amorphous glassy phase and crystalline phase, which can be considered

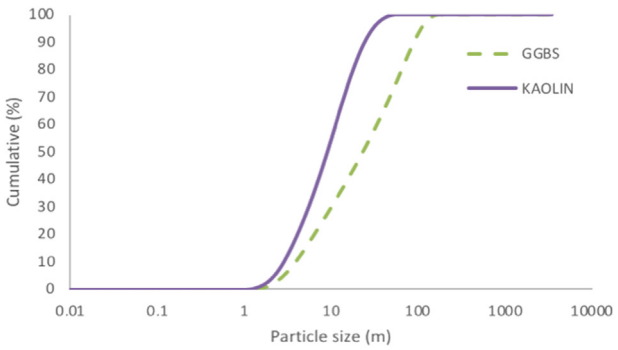

Fig. 2 – Particle size of kaolin and GGBS.

Table 1 – Chemical composition of raw kaolin and GGBS (wt%).

Chemical composition	CaO	SiO_2	Al_2O_3	Fe_2O_3	MgO	TiO_2	K_2O	ZrO_2	MnO_2	LOI
Kaolin	N/A	54.0	31.7	4.89	N/A	1.41	6.05	0.10	0.11	1.74
GGBS	50.37	30.4	10.5	0.53	3.2	0.98	N/A	0.05	0.71	0.32

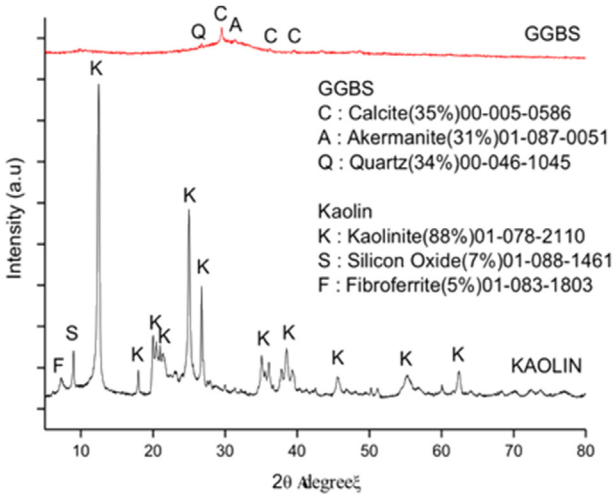

Fig. 3 – Phase composition of kaolin and GGBS.

as semi crystalline phase. The crystalline phase consisting of Calcite (CaCO3, ~35%), Akermanite (Ca2Mg(Si2O7), ~32%), and Quartz (SiO2, ~34%). The phase quantification was only for crystalline phases. The $CaCO_3$ and $Ca_2Mg(Si_2O_7)$ phases were in agreement with the high percentage of CaO in the chemical composition results of the GGBS.

Sharp peaks with high crystallinity and narrow peak bases are evident in the kaolinite phase at 2θ of ~13°, ~25°, and ~26°. The structure of kaolin, which is 1:1 layer of minerals, contain one tetrahedral and one octahedral sheet in their basic structural unit, as shown in Fig. 4. The sheets are held together by van der Waals bonds between the basal oxygens of the tetrahedral sheet and the hydroxyls of the octahedral sheet. The midplane of anions located within the two-layered sheets are strongly bonded via intermediate ionic-covalent bonds. The adjoining sheets are only loosely bound to one another via weak van der Waals forces. These double layers or sheets are stacked parallel to one another, forming a series of kaolinite crystals.

The layers are held together by hydrogen bonding, which restricts expansion and limits the reactive area to the external surfaces. Isomorphic substitution for Si^{4+} and Al^{3+} in this mineral is negligible. The crystalline form is more stable than the amorphous form, and reported lower energies at the molecular level with stronger bonds (mostly ionic bonds) between the molecules, which require more energy to break. This structural makeup explains the low reactivity properties of kaolin in geopolymerization mentioned in the literature.

The GGBS was in the amorphous state because of it had been quickly cooled off of the molten slag during the manufacturing process of pig iron. The bonding in amorphous has short range order and irregularly formed where the positions of individual atomic species are not randomly distributed in 3-D orientation. In other hand, amorphous commonly form in instable surface. Therefore, the addition of alkali activator will activated the surface of GGBS.

The FTIR spectrum in Fig. 5 shows that kaolinite has absorption bands within 3620–3696 cm^{-1}, corresponding to the stretching frequencies of the OH groups. The well-defined peak at this region confirms the ordered structure of kaolinite. However, this peak did not occur in GGBS due to its disordered structure, as per the XRD results. Another broad frequency at ~1451 cm^{-1} has been reported in the GGBS due to the asymmetric stretching of the CO_3^{2-} ion, indicating traces of carbonates [22]. characterized this band as the CO_3 stretching vibration mode caused by the presence of calcite due to the reaction between excess calcium

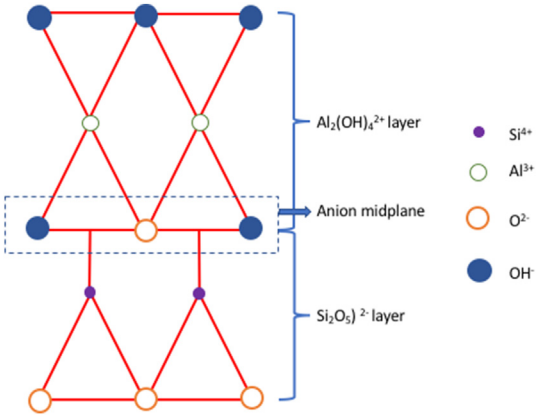

Fig. 4 – Structure of kaolin.

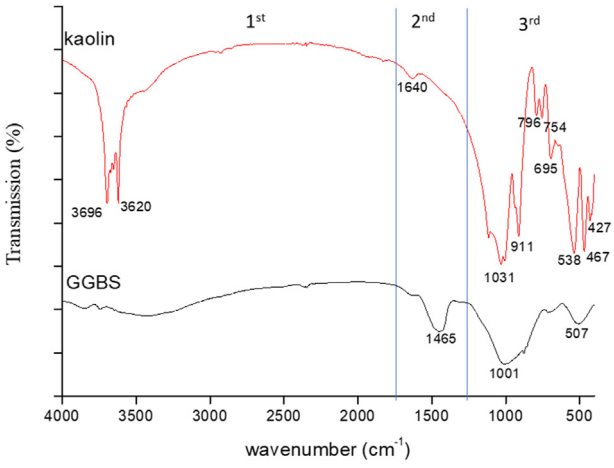

Fig. 5 – FTIR spectra of raw kaolin and GGBS.

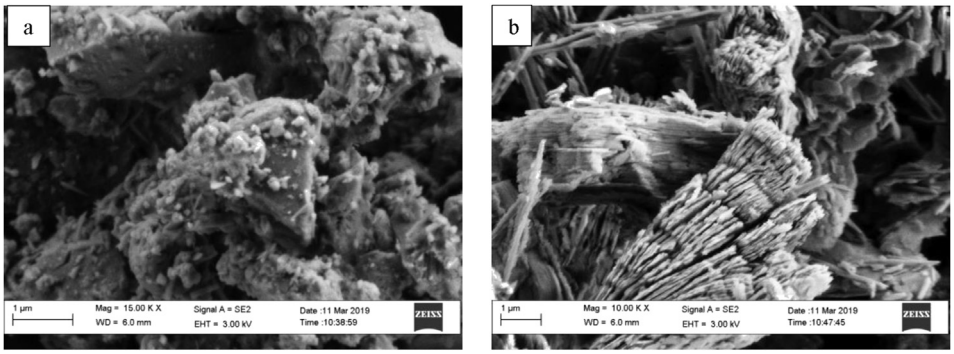

Fig. 6 – Microstructure of raw materials (a) GGBS and (b) kaolin.

oxide and atmospheric carbon dioxide. The ~35% calcite phase in the GGBS was evident in the XRD results.

The microstructure in Fig. 6(a) shows GGBS is flaky-shaped, with small spherical particles deposited onto the smooth larger surface, whilst (b) shows the layered structure of kaolin.

Fig. 7 shows the results of the thermal analysis of kaolin. The first endothermic peak of kaolin was observed at 50 - 200 °C. The mass loss at this initial endothermic peak is due to the release of physically-bound water. The second endothermic peak was observed at 500 - 600 °C, with ~8.72% of weight loss attributed to the loss of hydroxylated water bound to clay minerals and other volatile materials. >600 °C, almost all impurities in kaolin are expected to have volatized, resulting in flat TG curves.

Further heating kaolin to ~950 °C converts the metakaolin to a defective aluminum-silicon spinel ($Si_3Al_4O_{12}$), also referred to as a gamma-alumina type structure [18]. This occurrence was confirmed via the presence of a weak exothermic signal at ~1000 °C with no weight loss in the TG graph. The exothermic peak represents the formation of the crystalline phase. The weight change was verified by previous work to indicate the occurrence of dehydration due to the production of disordered metakaolin ($Al_2Si_2O_7$) [23].

The DTA curve for GGBS in Fig. 8 indicates a small exothermic peak at 600–800 °C, which is proportional to a mass loss ~0.96%. The small amount of weight loss is due to the properties of GGBS undergoing the dehydration process. An endothermic peak was evident at higher temperatures of 1100–1200 °C, indicating molecular rearrangement (glass crystallization). Based on the thermal analysis of kaolin and GGBS, two steps of the sintering profile were applied in order to decrease the cracking effect of the sintered samples with the heating profile.

3.2. *Effect of ratio solid to liquid on sintered kaolin-GGBS geopolymer*

3.2.1. *Chemical composition analysis*

Table 2 shows the chemical composition of the sintered kaolin-GGBS geopolymer. The chemical composition of the elements present in the sintered kaolin-GGBS geopolymer increased as the ratio of solid to liquid content increases, while the amount of Na_2O and SiO_2 in the sintered kaolin-GGBS geopolymer decreases as the solid-to-liquid ratio increases. This can be attributed to the amount of liquid consisting of the Na_2SiO_3 and NaOH in SL 2 being less than that in

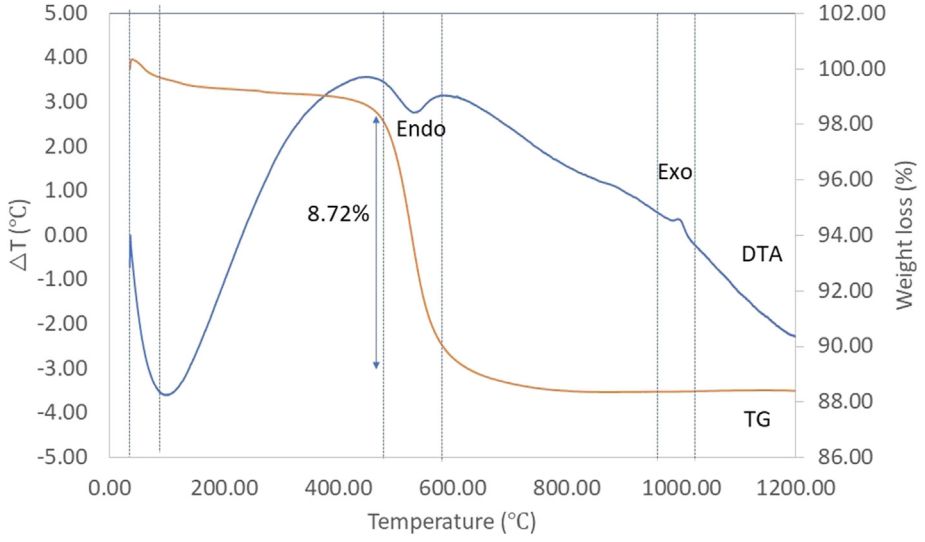

Fig. 7 – TG-DTA of kaolin.

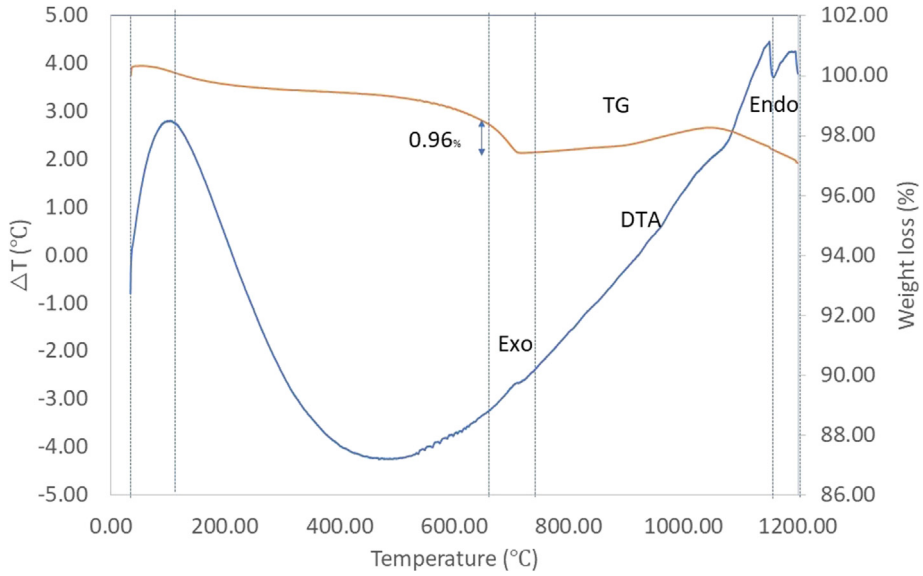

Fig. 8 – TG-DTA of GGBS.

Table 2 – Chemical composition of sintered kaolin-GGBS geopolymer with different ratio of solid to liquid.

Chemical composition	SL 1	SL 1.5	SL 2
Al_2O_3	17.9	20.3	21
CaO	6.62	7.33	8.44
Fe_2O_3	0.678	0.711	1
K_2O	2.99	3.37	3.35
MgO	0.971	1.05	1.39
TiO_2	0.334	0.367	0.43
Na_2O	6.13	4.71	4.1
SiO_2	64.1	61.7	59.6
LOI	67.09	73.63	77.48

SL 1. However, SiO_2 is also a major component in both kaolin and GGBS.

3.2.2. *Visual observation*

Fig. 9 was captured after unwrapped and partial demoulded the kaolin geopolymer after curing for 5 days in room temperature. The physical condition of kaolin geopolymer (without addition of GGBS) was not hardened but they were an improvement as the ratio of solid to liquid increase. The shape of kaolin geopolymer ratio of solid to liquid (SL 2) was still remain compared to the low ratio (SL 2).

The sintered kaolin-GGBS geopolymer is shown in Fig. 10. Although the kaolin-GGBS geopolymer was hardened at room temperature before sintering, visual observations shows the presence of visible microcracks in the surface of the sintered samples. The first step of sintering allowed for the slow release of H_2O, and the dihydroxylation reaction is expected to occur at higher temperatures due to increasing water pressure inhibiting dihydroxylation. Therefore, dihydroxylation prevented the initiation of cracks. Major cracking is defined as the total damage of the cubic sample post-sintering as shown in Fig. 11. The major cracking occur due to inadequate curing condition thus proceed to sintering.

3.2.3. *Microstructure analysis*

The micrograph in Fig. 12 shows the formation of the pores, which allows for a better understanding of the effects of the solid-to-liquid ratio on the sintered kaolin-GGBS geopolymer. SL 1, which contains the same proportion of solid and liquid, had larger cracks. The size of the massive pores of SL 1 shown

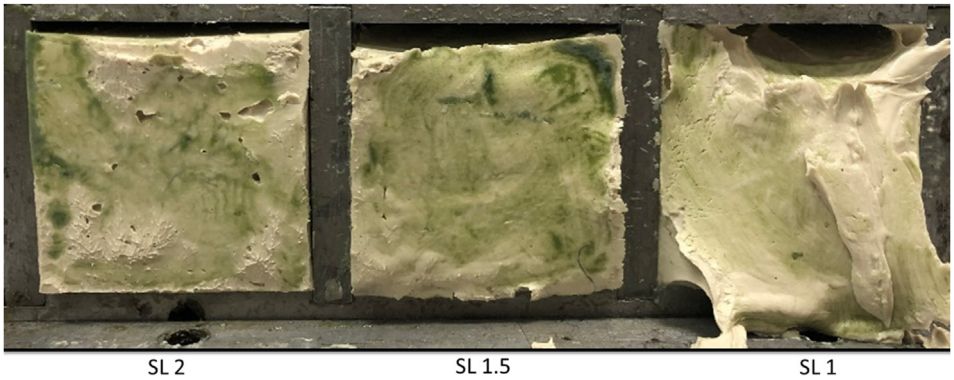

Fig. 9 – Physical condition of kaolin geopolymer after curing in room temperature for 5 days.

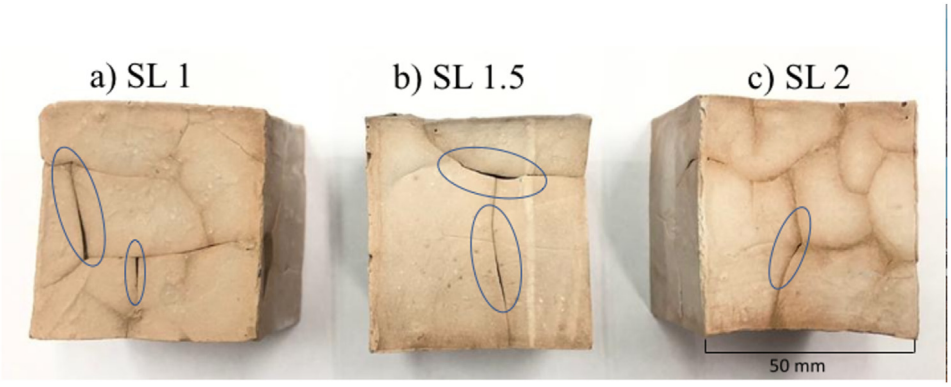

Fig. 10 – Visual observation on the visible cracks on the surface of sintered kaolin-GGBS geopolymer. (a) SL 1, (b) SL 1.5 and (c) SL 2.

Fig. 11 – Major cracking after two-steps of sintering of sintered kaolin-GGBS geopolymer due to inadequate curing condition.

in Fig. 12(a) were 2–5 um. It is an aggregation, forming a larger irregular and elongated formation with thin walls, as can be seen in the image. The formation of interconnected pores in SL 1 confirms the evaporation of water from the structure during sintering. The pressure in the movement of free water and hydroxylation during heating resulted in the formation of open pores due to the excessive water content in the geopolymer. The water did not only originated from alkali activator, but it was also due to the hygroscopic nature of kaolin itself.

The formation of two different regions was evident in the SL 1.5 sample. The regions are the densification region (A) and pores region (B), separated by an elongated crack. The crack seems to propagate as region A densified faster than region B. According to the EDX analysis, the amount of CaO in region A is ~31.48%, and it is ~8.78% in region B. The high amount of CaO was found to significantly affect the resulting hardened geopolymer. Furthermore, CaO increased the softening temperature and viscosity of the molten glass during sintering, thus making it harder for pores with smaller diameters to expand.

SL 2 shows a more densified region (similar to region A in SL 1.5), with well-defined pore formation relative to the other formulation. Most of the pores are closed, with different diameters. The amount of CaO in SL 2 is higher relative to that of the SL 1 due to the increased solid-to-liquid ratio. This could be due to when the surface energy function as a driving force and the solid kaolin-GGBS geopolymer begin forming sintering neck, it removes the entrapped air and decrease the presence of pores. Relative to SL 1 which reported low viscosity of molten glass due to its lower CaO content, SL 2 promoted the formation of pores due to its ease of movement and combination (creating larger pores). The pore distribution showed almost similar patterns with the ones reported in [24] at a ~55% addition of GGBS in the waste glass.

Research on the use of limestone ($CaCO_3$) dust as an additive in pottery clay shows positive impacts such as low water content in green bodies, which makes it easy to dry and reduce the energy expenditure required for firing. The results show that the shrinkage of samples post-drying is decreased when $CaCO_3$ content increases. When $CaCO_3$ is strongly heated, it will undergoes thermal decomposition to form calcium oxide (CaO) and carbon dioxide (CO_2). The drying shrinkage results confirms the evaporation of water from the green bodies, which is the main contribution of CaO towards the overall structure [25].

3.2.4. *Phase transformation analysis from XRD and FTIR result*

The semi-quantitative mineralogical estimation for each sample is presented in Fig. 13. Generally, the mixture of kaolin and GGBS as raw materials is activated by a suitable ratio of alkali activator, resulting in the formation of semi-crystalline sintered kaolin-GGBS geopolymer after undergoing the sintering process. As the ratio of solid-to-liquid increases, the degree of crystallinity decreases, as per the intensity of the peak. All reflections of the kaolinite phase in kaolin diminished post-sintering, reflecting the complete destruction of the crystal structure.

The free glass surfaces in the GGBS are preferable for devitrification, thus, crystallization could occur without the

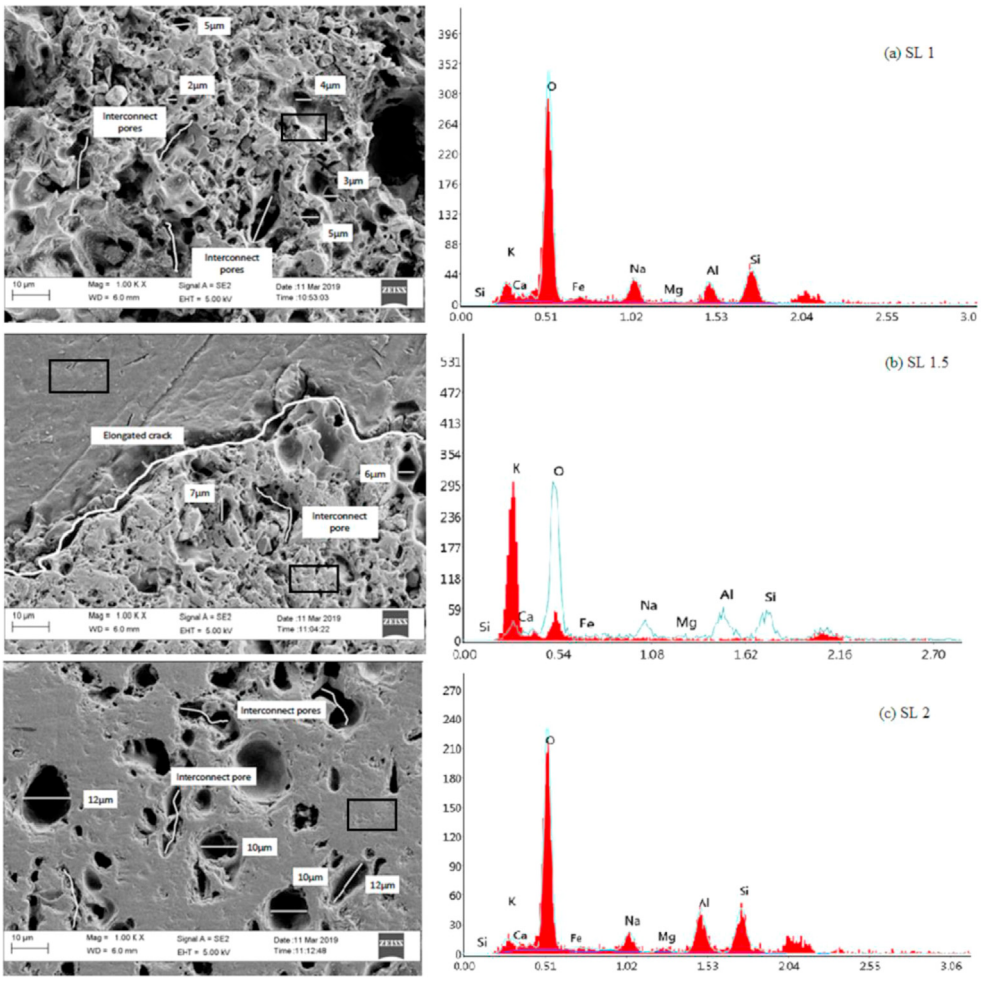

Fig. 12 – Microstructure of sintered kaolin-GGBS geopolymer and percentage of Ca from EDX analysis.

assistance of nucleating agents. The primary-precipitated phase of the GGBS will act as heterogeneous nucleating centres. During sintering, the main part of the crystalline phases corresponding to kaolin will disappear and be replaced by (new) amorphous and crystalline phases. This occurrence is an evident from the presence of the crystalline phase in kaolin diminishing post-sintering relative to the amorphous phase of slag. The quartz phase remain present in the sintered kaolin-GGBS geopolymer. However, changes in the intensity for the quartz phase in the sintered kaolin-GGBS geopolymer was observed. The increment/decrement intensities of the quartz phase is linked to the crystallization activity during sintering. The occurrence of the quartz phase in the GGBS decreased the firing shrinkage due to its acting like a skeleton during the formation of the liquid phase [30].

Quantitatively, the Nepheline phase, composed of Na, Al, Si, and O elements, was reduced from 84% in SL 1–61% in SL 1.5. It was further reduced to 13% post-sintering in the case of SL 2. These reductions are in agreement with the reduction of Na_2O and SiO_2 contents based on the chemical composition analyses of sintered kaolin-GGBS geopolymer shown in Table 2. The reduction of peak intensity means that the degree of crystallinity are distorted and amorphous as the solid content increases.

The solid-to-liquid ratio corresponds to the aluminosilicate-to-activator solution ratio. High solid content results in low viscosity of the kaolin-GGBS geopolymer slurry. The low liquid content was insufficient to activate geopolymerization in SL 2. Therefore, the excessive CaO and MgO from the GGBS do not contribute to the formation of a geopolymer network. However, the excessive ions react with SiO_2 to form the akermanite phase due to high reactivity of CaO and MgO based on the metal reactivity series. The akermanite phase consists of Ca, Mg, Si, and O, and its degree of crystallinity in SL 2 is higher than that of the akermanite in the GGBS.

New akermanite peak also was observed in the SL 2 at a diffraction angle of 16°. It was ascertained that the MgO induced the crystallization of the akermanite phase in SL 2. This occurrence was also confirmed via the disappearance of the gehlenite phase in SL 2 despite the increased gehlenite phase from SL 1 to SL 1.5. The elemental makeup in gehlenite include Ca, Al, Si and O. Gehlenite and akermanite both belong to the melilite group, which have excellent wear and corrosion resistances [4].

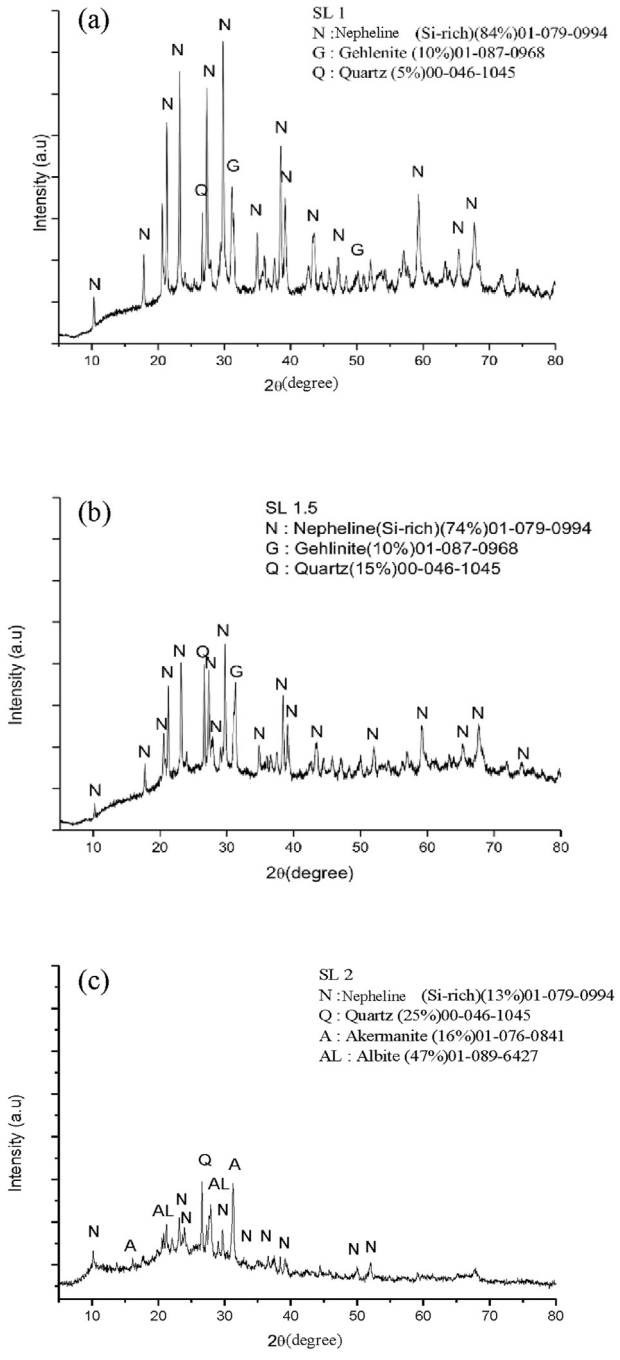

Fig. 13 – Phase composition of sintered kaolin-GGBS geopolymer with different solid to liquid ratio (a) SL 1, (b) SL 1.5 and (c) SL 2.

Another new phase occurring in the SL 2 is the albite, where it consist of Na, Al, Si, and O, at 47% as per the results of the semi-quantitative analysis. Although kaolin and GGBS have different crystallinity phases, it was confirmed that this aluminosilicate reacted during the phase transformation [26]. pointed out the interfacial energy between a glass and crystalline phase being higher between the two glassy phases. The phase differences could decrease the barrier to nucleation.

The considerable structural deformation caused by sintering was also confirmed in the FTIR results (Fig. 14). The

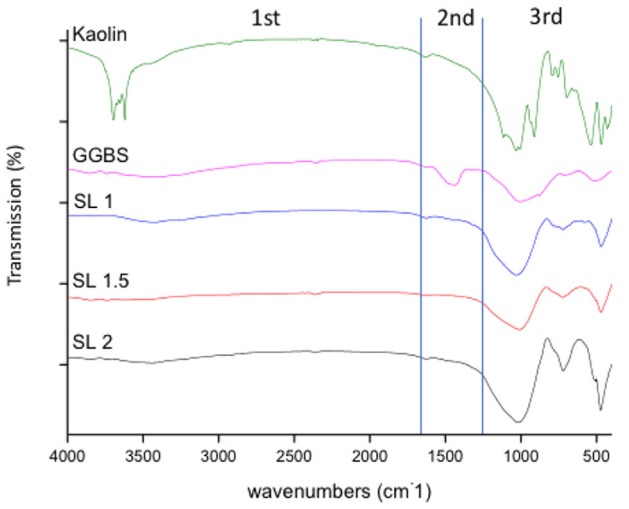

Fig. 14 – FTIR analysis indicates peak transformation of kaolin, slag and sintered kaolin-GGBS geopolymer at different ratio of solid liquid.

intensity of the 3600 cm^{-1} band diminished in the sintered kaolin-GGBS geopolymer, indicating the disordered structure due to dehydration caused by the formation of semi-crystalline phases in all of the sintered kaolin-GGBS geopolymer, as per the XRD results. This also proves that water was removed from the lattice post-sintering, which led to the disorientation of the crystal.

The second region (1300–1600 cm^{-1}) of the spectra shows only the 1451 cm^{-1} band in the GGBS. This band is assigned to the symmetric stretching mode of O–C–O bonds of carbonate group, which was subjected to superficial weathering of the GGBS during storage. The decomposition of $CaCO_3$ occurred at ~825 °C, as per [25]; which means that its linked to the disorientation of the carbonate band in the sintered kaolin-GGBS geopolymer.

The third region of the spectra located at 1300–400 cm^{-1} is also known as the fingerprint region. The Al–OH bending vibrations in kaolin at ~911 cm^{-1} disappeared in the geopolymer, implying the formation of asymmetric stretching of the Si–O–Si(Al) bridges around the 1000 cm^{-1} bands getting smoother in the sintered kaolin-slag geopolymer relative to that of the raw materials. This strongest vibration represents a major geopolymer fingerprint [20].

Post-sintering, the disappearance of the 911 cm^{-1} bands from the kaolin indicates the breakage of the Al–OH linkage. The alteration of the Si–O stretching and the disappearance of the Al–O–Si band indicate the distortion of the tetrahedral and octahedral layers. The decrease off the bonding energy of the OH groups in the sintered kaolin-GGBS geopolymer in the first region implies that the dehydration process during the first step of sintering at 500 °C is successful.

Disorientation is important as it allows for the kaolin to react with GGBS during geopolymerization. The breakage of the bonds will result in the imperfection of the crystal edges of kaolin. The electrophilic properties trap the hydroxyl groups in water, which correspond to the formation of silanol Si–OH and aluminol Al–OH groups at the kaolin platelets edges, which later fixes the cations in the solution. Besides the

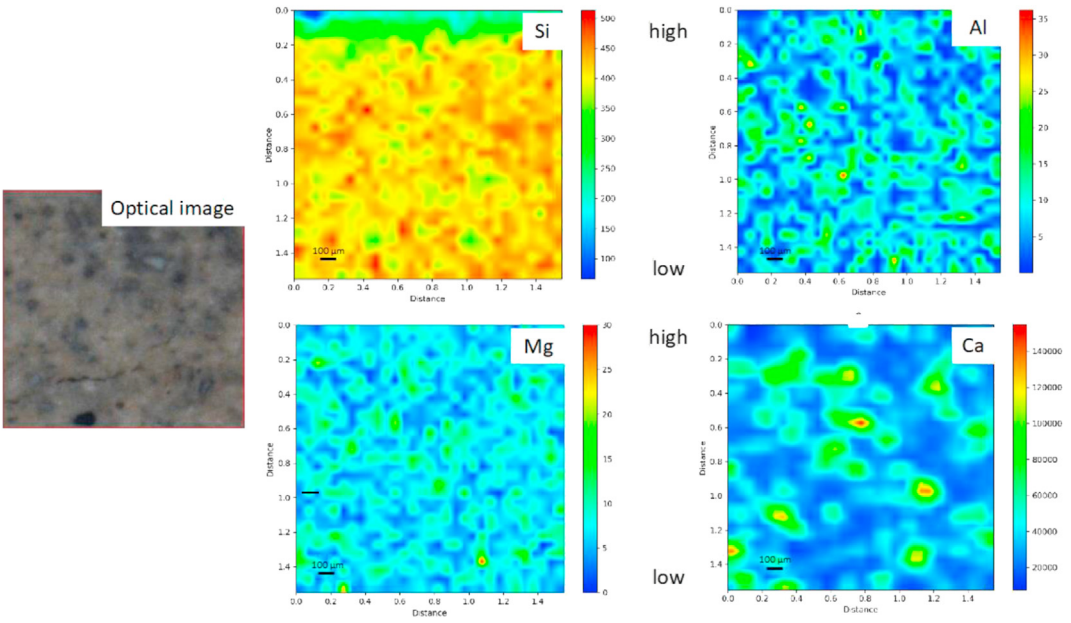

Fig. 15 – Optical image and micro-XRF elemental distribution maps of Si, Al, Mg and Ca of sintered kaolin-GGBS geopolymer with ratio of solid to liquid 2:1 (SL 2).

dihydroxylation of kaolin, the high alkalinity, which is indicative of high amounts of hydroxyl groups, changed the $[AlO]_6$ octahedral to $[AlO]_4$ tetrahedral. In this research, 8M of NaOH was used to achieve the abovementioned occurrence. The Si–O stretching at 695 cm^{-1} bands and the Al–SI–O stretching at 754 cm^{-1} in kaolin reacted during sintering to form the $[AlO]_4$ tetrahedra, confirmed by the 720 - 723 cm^{-1} transmittance peaks in the sintered kaolin-GGBS geopolymer. The transmission peak at 507 cm^{-1} in GGBS can be attributed to the bending vibration of the O–Si–O and Si–O–Si bond of the $[SiO]_4$ units.

3.2.5. *Elemental distribution from micro-XRF analysis*

Micro-XRF elemental maps shown in Fig. 15 were recorded in order to determine the distribution of Si, Al, Ca and Mg in sintered kaolin-GGBS. SL 2 was select for micro-XRF analysis due to the densification with regular pore distribution from the microstructure image. The colour bar indicates the concentration level of the elements which high concentration represent by reddish colour tone and blueish for low concentration. High concentration of Si shows homogenous distribution due to the phases (Nephaline, Quartz, Akermanite and Albite) presence in SL 2 consists of Si element. The distribution of Ca and Mg with high concentration in localized area reflects the akermanite phase. High concentration of Al indicates the phases of Nephaline and Albite.

4. Conclusion

In this study, kaolin (untreated) which have the main issue of low reactivity as a source material in geopolymer have react with the addition of GGBS. The effects of main chemical composition SiO_2, Al_2O_3, CaO and MgO on kaolin-GGBS geopolymer after sintering at 900 °C were studied. The phase transformation and microstructure based on different solid to liquid ratio were concluded:

1. The addition of GGBS to kaolin to form a geopolymer paste did not only accelerate the setting time of the geopolymer, it had contributed to the phase transformation of the sintered kaolin-GGBS geopolymer as well. High alkalinity of NaOH (8M) also influenced the structural changes of kaolin thus make it capable to react with GGBS.
2. As the solid-to-liquid ratio increases, the properties of the sintered kaolin-slag geopolymer changes accordingly. Highest solid content (SL 2) leads to the formation of new phases; akermanite and albite.
3. Two steps of sintering profile mitigated the initiation of cracks as the dihydroxylation mechanism is slowed, on top of phase transformation, the morphology of the sintered kaolin-GGBS geopolymer indicates an improved densification and pore formation with increasing solid-to-liquid ratio.

Declaration of Competing Interest

The authors declare that they have no known competing financial interests or personal relationships that could have appeared to influence the work reported in this paper.

Acknowledgments

The authors gratefully acknowledge the Centre of Excellent Geopolymer and Green Technology, (CeGeoGTech), UniMAP for the financial support. The authors would like to extend

their gratitude to the (CeGeoGTech), UniMAP for the financial support. The authors would like to extend their gratitude to the European Union for sponsoring the "Partnership for Research in Geopolymer Concrete" (PRI-GeoC-689857) grant under H2020 Marie Sklodowska-Curie Rise by European Commission. A special thanks is dedicated to Synchrotron Light Research Institute (SLRI), Thailand for essential testing accommodation.

REFERENCES

[1] Bai C, Li H, Bernardo E, Colombo P. Waste-to-resource preparation of glass-containing foams from geopolymers. Ceram Int 2019;45(6):7196–202.
[2] Rincón A, Desideri D, Bernardo E. Functional glass-ceramic foams from 'inorganic gel casting' and sintering of glass/slag mixtures. J Clean Prod 2018;187:250–6. https://doi.org/10.1016/j.jclepro.2018.03.065.
[3] Villaquirán-Caicedo MA, de Gutiérrez RM. Synthesis of ceramic materials from ecofriendly geopolymer precursors. Mater Lett 2018;230:300–4.
[4] Liu H, Lu H, Chen D, Wang H, Xu H, Zhang R. Preparation and properties of glass-ceramics derived from blast-furnace slag by a ceramic-sintering process. Ceram Int 2009;35(8):3181–4. https://doi.org/10.1016/j.ceramint.2009.05.001.
[5] Zhang ZH, Zhu HJ, Zhou CH, Wang H. Applied clay science geopolymer from kaolin in China : an overview. Appl Clay Sci 2016;119:31–41. https://doi.org/10.1016/j.clay.2015.04.023.
[6] Koleżyński A, Król M, Żychowicz M. The structure of geopolymers – theoretical studies. J Mol Struct 2018;1163:465–71. https://doi.org/10.1016/j.molstruc.2018.03.033.
[7] Wei YL, Weng S, Di, Xie XQ. Reduction of sintering energy by application of calcium fluoride as flux in lightweight aggregate sintering. Construct Build Mater 2018;190:765–72. https://doi.org/10.1016/j.conbuildmat.2018.09.134.
[8] Nath P, Sarker PK. Effect of GGBFS on setting, workability and early strength properties of fly ash geopolymer concrete cured in ambient condition. Construct Build Mater 2014;66:163–71.
[9] Heah CY, Kamarudin H, Mustafa Al Bakri AM, Bnhussain M, Luqman M, Khairul Nizar I, Liew YM. Study on solids-to-liquid and alkaline activator ratios on kaolin-based geopolymers. Construct Build Mater 2012;35:912–22. https://doi.org/10.1016/j.conbuildmat.2012.04.102.
[10] Hounsi AD, Lecomte-Nana GL, Djétéli G, Blanchart P. Kaolin-based geopolymers: effect of mechanical activation and curing process. Construct Build Mater 2013;42:105–13. https://doi.org/10.1016/j.conbuildmat.2012.12.069.
[11] Wan Q, Rao F, Song S. Reexamining calcination of kaolinite for the synthesis of metakaolin geopolymers-roles of dehydroxylation and recrystallization. J Non-Cryst Solids 2017;460:74–80.
[12] Papa E, Medri V, Amari S, Manaud J, Benito P, Vaccari A, Landi E. Zeolite-geopolymer composite materials: production and characterization. J Clean Prod 2018;171:76–84. https://doi.org/10.1016/j.jclepro.2017.09.270.
[13] Škvára F, Šmilauer V, Hlaváček P, Kopecký L, Cilova Z. A weak alkali bond in (N, K)–A–S–H gels: evidence from leaching and modeling. Ceramics–Silikáty 2012;56(4):374–82.
[14] Lee WH, Wang JH, Ding YC, Cheng TW. A study on the characteristics and microstructures of GGBS/FA based geopolymer paste and concrete. Construct Build Mater 2019;211:807–13. https://doi.org/10.1016/j.conbuildmat.2019.03.291.
[15] Heah CY, Kamarudin H, Mustafa Al Bakri AM, Bnhussain M, Luqman M, Khairul Nizar I, Liew YM. Kaolin-based geopolymers with various NaOH concentrations. Int J Miner Metallurg Mater 2013;20(3):313–22. https://doi.org/10.1007/s12613-013-0729-0.
[16] Naghsh M, Shams K. Synthesis of a kaolin-based geopolymer using a novel fusion method and its application in effective water softening. Appl Clay Sci 2017;146:238–45.
[17] Okoye FN, Durgaprasad J, Singh NB. Mechanical properties of alkali activated flyash/Kaolin based geopolymer concrete. Construct Build Mater 2015;98:685–91.
[18] Wang W, Liu H, Gu W. A novel fabrication approach for improving the mechanical and sound absorbing properties of porous sound-absorbing ceramics. J Alloys Compd 2017;695:2477–82. https://doi.org/10.1016/j.jallcom.2016.11.147.
[19] Tippayasam C, Keawpapasson P, Thavorniti P, Panyathanmaporn T, Leonelli C, Chaysuwan D. Effect of Thai Kaolin on properties of agricultural ash blended geopolymers. Construct Build Mater 2014;53:455–9.
[20] Ye J, Zhang W, Shi D. Effect of elevated temperature on the properties of geopolymer synthesized from calcined ore-dressing tailing of bauxite and ground-granulated blast furnace slag. Construct Build Mater 2014;69:41–8. https://doi.org/10.1016/j.conbuildmat.2014.07.002.
[21] Sudbrink B, Moradllo MK, Hu Q, Ley MT, Davis JM, Materer N, Apblett A. Imaging the presence of silane coatings in concrete with micro X-ray fluorescence. Cement Concr Res 2017;92:121–7.
[22] Davidovits J. Geopolymer cement. a review, vol. 21. Geopolymer Institute; 2013. p. 1–11. Technical papers.
[23] Yaya A, Tiburu EK, Vickers ME, Efavi JK, Onwona-Agyeman B, Knowles KM. Characterisation and identification of local kaolin clay from Ghana: a potential material for electroporcelain insulator fabrication. Appl Clay Sci 2017;150(March):125–30. https://doi.org/10.1016/j.clay.2017.09.015.
[24] Ding L, Ning W, Wang Q, Shi D, Luo L. Preparation and characterization of glass-ceramic foams from blast furnace slag and waste glass. Mater Lett 2015;141:327–9. https://doi.org/10.1016/j.matlet.2014.11.122.
[25] Sangsuk S, Khunthon S, Saenapitak S. Effect of limestone dust on the properties of Thai pottery sintering at low temperature 2008;18(1):1–7.
[26] Khater GA. The use of Saudi slag for the production of glass-ceramic materials. Ceram Int 2002;28(1):59–67. https://doi.org/10.1016/S0272-8842(01)00058-X.
[27] Liu J, Yu Q, Zuo Z, Yang F, Han Z, Qin Q. Reactivity and performance of dry granulation blast furnace slag cement. Cement Concr Compos 2019;95:19–24.
[28] Hounsi AD, Lecomte-Nana G, Djeteli D, Blanchart P, Alowanou D, Kpelaou P, et al. How does Na, K alkali metal concentration change the early age structural characteristic of kaolin-based geopolymers. Ceramics International 2014;40(7):8953–62. https://doi.org/10.1016/j.ceramint.2014.02.052.
[29] Hongyu L, Hongxia L, Deliang C, Hailonh W, Hongliang X, Rui Z. Preparation and properties of glass-ceramics derived from blast-furnace slag by a ceramic-sintering process. Ceramics International 2009;35(8):3181–4. https://doi.org/10.1016/j.ceramint.2009.05.001.
[30] Alves HP, Silva JB, Campos LF, Torres SM, Dutra RP, Macedo DA. Preparation of mullite based ceramics from clay–kaolin waste mixtures. Ceramics international 2016;42(16):19086–90.